AIChE

Optimizing the Rotated Arc Mixer

Mrityunjay K. Singh and Patrick D. Anderson
Dept. of Mechanical Engineering, Materials Technology, Eindhoven University of Technology, 5600 MB Eindhoven, The Netherlands

Michel F. M. Speetjens
Dept. of Mechanical Engineering, Energy Technology, Eindhoven University of Technology, 5600 MB Eindhoven, The Netherlands

Han E. H. Meijer
Dept. of Mechanical Engineering, Materials Technology, Eindhoven University of Technology, 5600 MB Eindhoven, The Netherlands

DOI 10.1002/aic.11586
Published online September 26, 2008 in Wiley InterScience (www.interscience.wiley.com).

Using the mapping method an efficient methodology is developed for mixing analysis in the rotated arc mixer (RAM). The large parameter space of the RAM leads to numerous situations to be analyzed to achieve best mixing, and hence, it is indeed a challenging task to fully optimize the RAM. Two flow models are used to study mixing: one based on the full three-dimensional (3-D) flow field, and a second one based on a simplified 2.5-D model, where an analytical solution is used for transverse velocity components in combination with a Poiseuille profile for the axial velocity component. Detailed 3-D velocity field analyses reveal locally significant deviations from the Poiseuille profile e.g., presence of back-flow, but only minimal differences in mixing performance is found using both flow models (3- and 2.5-D) in the RAM designs that are candidates for accomplishing chaotic mixing. Despite the computational advantage of the 2.5-D approach over the 3-D approach, it is still cumbersome to analyze mixing for large number of designs using techniques based on particle tracking, e.g., Poincaré sections, dye traces, stretching distributions. Therefore, in this respect the mapping method provides an engineering tool able to tackle this optimization problem in an efficient way. On the basis of mixing evaluations, both in qualitative and quantitative sense, for the whole range of parameter space, the optimum set of design and kinematical parameters in the RAM is obtained to accomplish the best mixing. *AIChE J,* 54: 2809–2822, 2008
Keywords: mixing, chaos, mapping, optimization, rotated arc mixers

Introduction

Mixing of fluids is an important process in many industrial operations and devices. Turbulence is an important candidate to achieve excellent mixing in short time scales, but it is absent in various homogenization processes given the high viscosity of processed materials, which leads to laminar flow. Laminar flow can also produce irregular trajectories of fluid particles, resulting in efficient mixing via chaotic advection.[1,2] The principles of chaotic advection, which mimics the Bakers transformation: a continuous repetition of stretching and folding, are harnessed in many industrial continuous mixers for viscous fluids. Examples include the Kenics mixer,[3] the multiflux mixer,[4] the SMX mixer,[5] various

Correspondence concerning this article should be addressed to P. D. Anderson at p.d.anderson@tue.nl.

extruders, and a more recent development, the rotated arc mixer (RAM).[6–8] All the above mixers fall in the category of so-called reoriented duct flows, which consist of an uniaxial flow, a transverse flow perpendicular to the axial flow, and a systematic reorientation of this transverse flow. This reorientation results in the crossing of transverse streamlines at different spatial positions, eventually yielding chaotic mixing.

In this study, we focus on mixing analyses and full optimization of the RAM. The RAM consists of two snugly fit concentric cylinders—the outer one is rotating and the inner one is stationary. The inner cylinder contains a sequence of open windows in the axial direction that are offset with respect to its neighboring windows along the circumference. As fluid flows through the inner cylinder, the outer cylinder rotation induces transverse flow through viscous drag at the open windows. The offset of these windows provides crossing streamlines at different axial positions. Key parameters that determine the quality of mixing in a RAM are: opening angle of windows (Δ), offset angle (Θ), and a dimensionless kinematical parameter $\beta = \omega L/\langle v \rangle$, where ω is rotation speed of the outer cylinder, L is the length of the window, and $\langle v \rangle$ is the average axial velocity. Physically the dimensionless kinematical parameter β is the cross-sectional stretching per window residence time. Tuning of these three parameters (Δ, Θ, β) is essential to obtain chaotic mixing in the device and involves a large parameter space to be analyzed,[6] and hence, it is a daunting task to fully optimize the RAM.

Metcalfe et al.[6] used a number of numerical techniques (Poincaré sections, dye traces, and stretching distributions) to characterize the quality of mixing in the device, and suggested a numerical sieving procedure to find an optimum range of parameters. They suggested that the computationally least expensive techniques can be used to refine the search space followed by analyzes using the expensive tools in this refined parameter space. In the three-dimensional (3-D) geometry of the RAM, the general strategy followed is to determine a 3-D velocity field, and subsequently tracking passive tracers in the flow field to find the final distributions and statistics of tracers (we call this the 3-D approach). Metcalfe et al.[6] reported that the huge computational cost can be reduced by considering the in-plane analytic solution of Hwu et al.[9] for the transverse components of the velocity in the Stokes flow regime for Newtonian fluids, and assuming Poiseuille profile for the axial velocity to track tracer positions in the flow field (we call this the 2.5-D approach). This approach is fast because during tracking all the three velocity components are available analytically. However, the drawback of this 2.5-D approach is that it does not take into account the transitional effects produced by reorientation of flow between two consecutive windows, which may create significant differences in mixing profiles. A detailed analysis is needed before relying on this approach. For example, in the partitioned pipe mixer, it has been found that the transition regions play an important role in deciding the fate of KAM (Kolmogorov–Arnold–Moser) boundaries,[10] and therefore, it is important here to investigate the transition effects in the RAM.

Our main objective is to develop an efficient methodology for mixing analysis in the mixer, and consequently, find the complete optimized parameter space for which the RAM has its best mixing performance (in the Stokes regime for Newtonian fluids). It is apparent that to reduce computation times, the 2.5-D approach should be exploited, but as mentioned earlier it raises some serious doubts whether the conclusions drawn from the two approaches, 2.5- and full 3-D, are the same or different. To address this issue in detail, we will use a direct comparison of 2.5- to 3-D velocity fields as well as mixing profiles obtained by these flow fields. We will report on the region where the 2.5-D is valid, i.e. where the differences between mixing profiles of both approaches are insignificant. Although the 2.5-D approach drastically reduces computation time, the analysis of the complete parameter space is still a challenging task by the techniques mentioned in previous studies of the RAM.[6–8] This is due to various facts. First, any change in a design or kinematical parameter requires a re-computation of all tracking results. Second, the tracking procedure must be repeated for all windows of the RAM involved in mixing. Finally, the large parameter space requires analyzing numerous cases. Moreover, mixing analyses by the 3-D approach necessitates a recomputation of both velocity field and tracking results with any change in parameter, which augments the computational cost. Besides, in most cases back-flows (negative axial velocity) exist in the 3-D velocity field, which further complicates the tracking of tracers. All this leads to one conclusion: the requirement of computationally more advantageous approaches to tackle this type of optimization problems. We will demonstrate in this article that the mapping method[11–16] indeed provides a solution to this problem, and it can be utilized as an efficient tool to study in-depth mixing in RAM, and subsequently to find the optimized set of design and kinematical parameters of the RAM in an efficient way. In the mapping method, the deformation history of fluids due to a specified flow is stored in the form of a distribution matrix, subsequently allowing evaluation of the effect of the flow during any number of cycles by a repeated multiplication of the distribution matrix with a prescribed concentration vector at the inlet. In addition, the mapping method provides quantitative mixing measures like the intensity of segregation and the scale of segregation to judge the quality of a mixer.

The article is organized as follows. First, we start with explaining the problem at hand, and second we present a detailed analysis of the flow field in the RAM. Third, we describe the method to analyze mixing where we introduce the mapping method. Finally, we summarize the most relevant outcomes of our mixing analyses and draw conclusions.

Problem Definition

The four important geometrical parameters Δ, Θ, L, and R are defined as shown in Figure 1, where Δ is the opening angle of a window, Θ the offset angle of subsequent windows along the circumference (with respect to origin), L the axial length of a window, and R the radius of the cylinder. It is convenient to define the kinematical parameter β, related to the operational parameter, incorporating L, and R as follows:

$$\beta = \frac{(\omega R)L}{(\langle v \rangle)R} = \frac{L\omega}{\langle v \rangle} \tag{1}$$

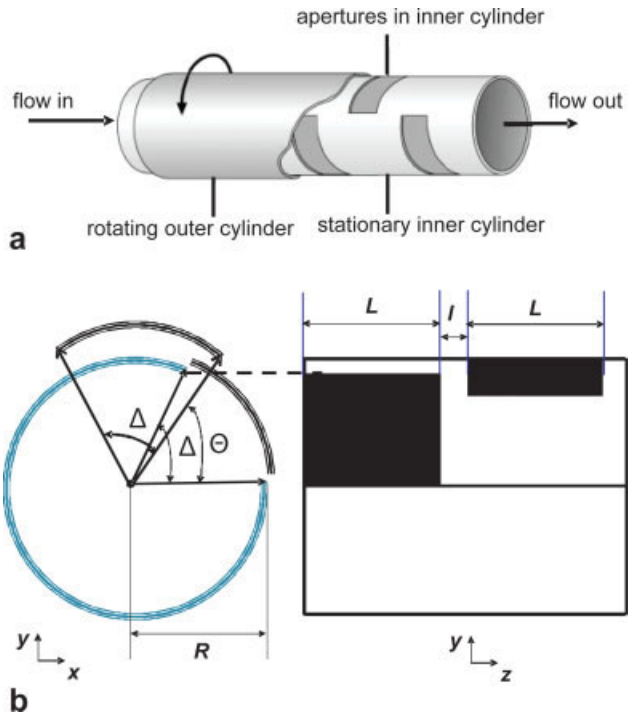

Figure 1. Defining geometrical parameters of RAM.

(a) Schematic of the rotated arc mixer (adopted from Metcalfe et al.[6]), (b) cross-sectional and axial view, respectively, showing geometric parameters, Δ is spawn angle of an window along the periphery, Θ is offset angle between two consecutive windows, R the radius of the cylinder, L the axial length of a window, and l the axial distance (gap) between two consecutive windows (black area showing the opening of windows). [Color figure can be viewed in the online issue, which is available at www.interscience.wiley.com.]

where $\langle v \rangle$ is the average inlet velocity, and ω is rotation speed of the cylinder. Finally, the number of windows N_w is also an important design parameter that decides the final quality of mixing. In this study, we fix this parameter at 10. The geometrical parameter Δ can vary in the range of $[-360, 0]$ degrees (note that sign of Δ does not effect final quality of mixing), whereas Θ covers the range $[-180,180]$ degrees. We cover the offset angle (Θ) range starting from negative to positive, because the way of offset relative to the rotation direction ω is crucial for the final quality of mixing.[6,7] Reversing ω is equivalent to substituting $\Theta \rightarrow -\Theta$,[6,7] and in this study, the $-\Theta$ is always achieved by changing the sign of the ω. The kinematical parameter β covers the total range $[0, \infty]$. When β approaches zero, ω approaches zero, and hence, this will lead to a simple pipe flow situation. The other extreme, where β approaches infinity, is realized either by decreasing $\langle v \rangle$ down to zero or by applying a very high rotational speed. The first case ($\langle v \rangle \rightarrow 0$) gives almost zero throughput, whereas the second case ($\omega \rightarrow \infty$) finds practical limits, and could be expensive. Therefore, we fix the range of β to [0, 30], because Metcalfe et al.[6] and Speetjens et al.[7] found that this range admits chaotic advection. To change β one can change L or ω, and changing L requires remeshing the new design, therefore changes in ω are preferred. To optimize the RAM, it is required to investigate the effects of all three parameters [Δ, Θ, β]. In this article, the mixing measure intensity of segregation I_d, obtained from the mapping method, is used as an objective function to quantify the effect of all three parameter spaces [Δ, Θ, β] (for details of intensity of segregation see "Methods to Analyze Mixing" section).

Flow Field Calculations

The RAM flow field consists of three velocity components. The two transverse components of the velocity, $\boldsymbol{u_x}$ and $\boldsymbol{u_y}$ in the cartesian coordinate system ($\boldsymbol{u_r}$ and $\boldsymbol{u_\theta}$ in the cylindrical co-ordinate system), emanate from viscous drag imparted by the outer rotating cylinder at open windows of inner stationary cylinder, and the axial velocity component $\boldsymbol{u_z}$ is induced by the pressure difference along the duct. The coupling between transverse and axial components requires computation of the full 3-D velocity field (3-D approach). If this coupling is weak, 2.5-D approach may be employed. Note that the main reason to use the 2.5-D approach is that if it is valid then this leads to a huge reduction in computational effort to analyze mixing for various cases. Therefore, we investigate both options.

Velocity field: 2.5-D approach

Hwu et al.[9] derived an analytical solution for 2-D steady Stokes flow in a circular cavity induced by movable arcs along a circular sidewall, yielding transverse components of the velocity ($\boldsymbol{u_x}$ and $\boldsymbol{u_y}$ or $\boldsymbol{u_r}$ and $\boldsymbol{u_\theta}$) in the case of weak coupling. The axial velocity component $\boldsymbol{u_z}$ is found from the Hagen–Poiseuille solution for pipe flow (parabolic velocity profile). In this way, all the velocity components are analytically known for a window of the RAM. To obtain velocity components for subsequent windows, this velocity field is reoriented by the offset angle (Θ) and leads to an overall reoriented cellular flow model of the RAM. The global flow field of RAM for the 2.5-D approach can be expressed as follows:

$$\boldsymbol{u_{xy}}(\boldsymbol{r}, \boldsymbol{\theta}, z) = \boldsymbol{u_{xy}}(\boldsymbol{r}, \boldsymbol{\theta} - \boldsymbol{\theta_R}(z), z), \quad \boldsymbol{u_z} = \boldsymbol{u}(\boldsymbol{r}, \boldsymbol{\theta}), \qquad (2)$$

where $\boldsymbol{\theta}_R(z) = \Theta \sum_{i=1}^{N_w} H(z - iL)$ is the reorientation angle, H the Heaviside function, θ the azimuthal component of the cylindrical frame of reference (r, θ, z), and L the length of a window. In other words, if the velocity field ($\boldsymbol{u_x}$, $\boldsymbol{u_y}$, $\boldsymbol{u_z}$) is known for a window at a point (x, y, z), then the velocity field for the consecutive window at a point (x, y, $z + L$) can simply be obtained by rotational transformation. This rotational transformation can be applied to obtain the velocity field at any desired location in the RAM. Thus, only the velocity field within the first window must be computed; the velocity field at subsequent windows simply follows from reorientation of the field at the first window.

Velocity field: 3-D approach

To resolve the issues related with entrance and exit effects at each window and characterize coupling in the velocity field, we perform full 3-D computations of velocity field in the RAM with 10 windows. The geometry used to obtain 3-D velocity fields are as follows: radius $R = 4.4$ cm, length

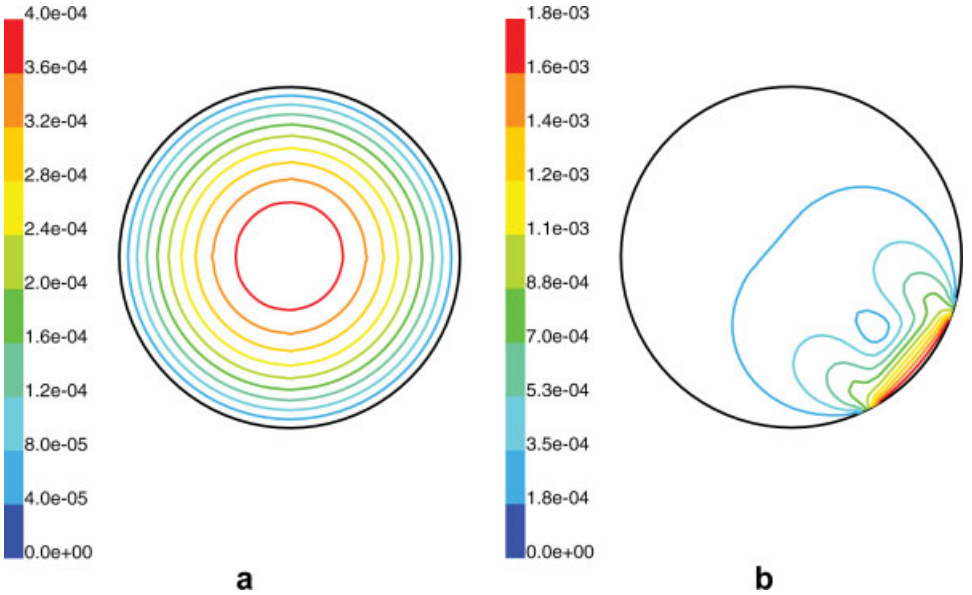

Figure 2. Typical 3-D flow field in the RAM for $\beta = 20$ at middle of the window, (a) axial velocity u_z and (b) magnitude of transverse velocity $|u_{xy}| = (u_x^2+u_y^2)^{1/2}$.

[Color figure can be viewed in the online issue, which is available at www.interscience.wiley.com.]

of a window $L = 10$ cm, axial gap between two neighboring windows $l = 1$ cm, opening angle $\Delta = 45^\circ$, and offset angle $\Theta = -36^\circ$ adopted from Metcalfe et al.[6] (see Figure 1). The kinematical parameter β is varied in the range [1, 30]. A structured hexahedral mesh is obtained with Gambit V2.1.2 (number of nodes = 561,275, number of cells = 548,000), and Fluent V6.1.22 is used to obtain the 3-D velocity field. The fluid is assumed to be Newtonian and incompressible with density $\rho = 1230$ kg/m^3 and viscosity $\mu = 1.5$ kg m/s. For velocity field computations, periodic boundary conditions are prescribed between inlet and outlet and at the inlet a mass flow rate $\dot{m} = 1.495 \times 10^{-3}$ kg/s is imposed. The Reynolds number, Re $(=\rho u D/\mu$, where D is diameter), is below 10^{-2} for all simulations. Hence, the flow is clearly in the Stokes regime.

Figure 2 displays a typical flow field of the RAM, where contours of axial velocity $\boldsymbol{u}_z$ and magnitude of transverse velocity $|\boldsymbol{u}_{xy}| = (\boldsymbol{u}_x^2+\boldsymbol{u}_y^2)^{1/2}$ are shown at the middle of a window. The axial profile $\boldsymbol{u}_z$, as shown in Figure 2a, has nearly an axis-symmetric shape, almost a Poiseuille profile. The transverse velocity $|\boldsymbol{u}_{xy}|$, as shown in Figure 2b reveals transverse circulation set up by the moving boundary at open window, the large transversal velocities occurring at moving boundaries. Figure 3a shows the contour plots of the axial velocity for $\beta = 20$ at three different locations of a window, the first contour is plotted at the left side of the window, the second in the middle, and the third between two windows. In the middle of the window, the Poiseuille profile prevails, while when fluid approaches the entrance of the window (left side contour) or even surpassing the exit of window (right contour) deviations occur from the Poiseuille profile, as demonstrated by the presence of negative axial values (backflow), and revealed by distorted contour lines. Note that presence of negative velocities excludes the option of axial tracking approach and it requires time-tracking approach. This will be discussed in detail in the next section. To characterize deviations in the velocity field at various cross-sections of a window with respect to middle of the window, we define a deviation parameter:

$$\boldsymbol{\delta u} = \sqrt{\frac{1}{N}\sum_{i=1}^{N}\left|\boldsymbol{u}^i - \boldsymbol{u}_0^i\right|^2}, \tag{3}$$

where $\boldsymbol{u}^i$ and $\boldsymbol{u}_0^i$ are the velocity components at the same cross-sectional location (point number i) in the disturbed (away from the middle of a window), and undisturbed (at the middle of a window) velocity field, on a grid of $N = 10{,}000$ points, distributed evenly over the cross-section. Figure 3b shows the deviation $\boldsymbol{\delta u}$ for the axial velocity component $(\boldsymbol{\delta u}_z)$, scaled with the average axial velocity $\langle v\rangle$, for $\beta = 20$ and 30. The larger $\boldsymbol{\delta u}_z$ the stronger is the coupling in velocity field. Assuming that 10% deviations from Poiseuille profile is less severe, this plot reveals that at $\beta = 20$ and $\beta = 30$ approximately 40 and 60%, respectively, of a window is involved in the transition region. The deviation $\boldsymbol{\delta u}_z$ is found to decrease for lower values of β. The back flow only starts to appear upon exceeding a critical β, and is found in the vicinity of the edges of the window covering some region along the window as well as extending into the gap between two neighboring windows. Figure 4 characterizes the effect of β on maximum negative axial velocity $\boldsymbol{u}_z$, scaled with $\langle v\rangle$. Back flow (negative $\boldsymbol{u}_z$) starts to appear for $\beta > 4$ (critical β), and its maximum magnitude approaches $\langle v\rangle$ when $\beta \approx 20$. The negative flux that is carried by back flow normalized with the total flux is given in Figure 4b as a function of β. An increase in β leads to a higher value of negative as well as a higher area coverage by the back flow (at the exit cross-

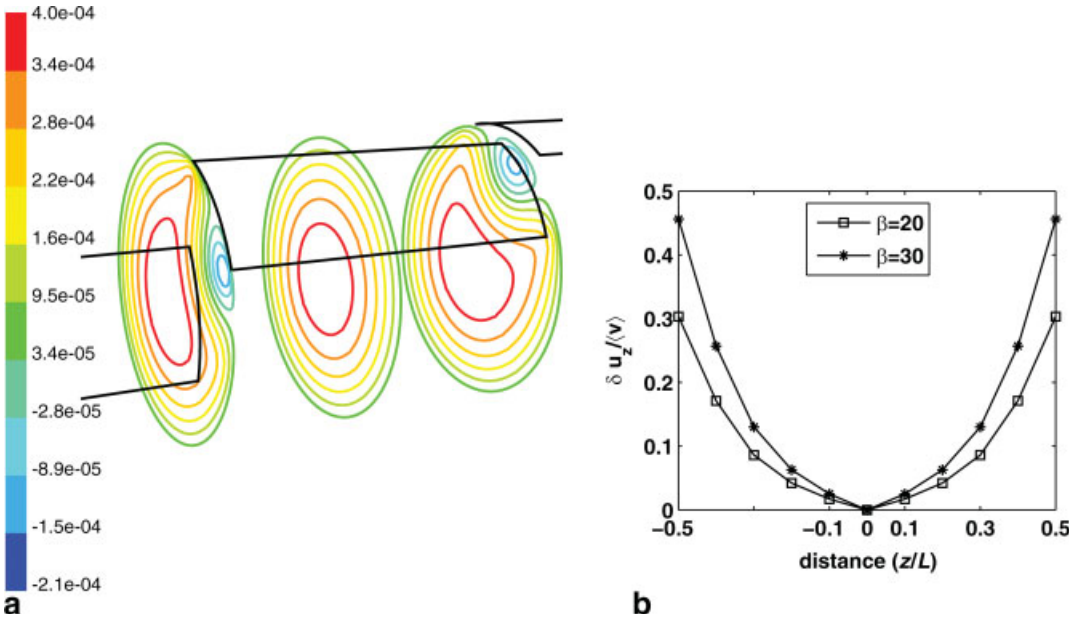

Figure 3. Characterizing entrance and exit effects of a window: deviations in axial velocity field from the Poiseuille profile in a window of the RAM.

(a) Axial velocity contour plots for $\beta = 20$, and (b) finding how intense the deviations from Poiseuille flow exists along a window for $\beta = 20$ and 30, the deviations $\boldsymbol{\delta u}_z$ are computed with respect to axial velocity from middle of the window ($z/L = 0$ at middle of the window, L is length of a window, negative ($-$) and positive distance is left and right, respectively, from middle of the window). [Color figure can be viewed in the online issue, which is available at www.interscience.wiley.com.]

section of a window) with a negative flux of maximum 5% of the total flux at highest $\beta = 30$. The preceding analyses proved that a pronounced coupling in transverse and axial velocity components exist especially at higher values of β.

Even though there exists a strong coupling in the 3-D flow field, the detailed analysis of the velocity field reveals that the 3-D flow field has the same spatial periodicity as the 2.5-D flow field, the 3-D flow field can be expressed in terms of reoriented cellular flow model. This can be verified by comparing velocity fields of two consecutive neighboring windows in the following way: reorient the velocity field obtained at a cross-sectional position z of a window by the offset angle Θ (rotational transformation as mentioned for 2.5-D) and then compute the deviation in velocity $\boldsymbol{\delta u}$ (Eq. 3) with respect to the velocity field obtained at cross-sectional position $z + L + l$ of the next neighboring window. If the cellular flow model is valid, then this deviation $\boldsymbol{\delta u}$ must approach zero. In this manner, we compute the deviations ($\boldsymbol{\delta u}$) for all the components of velocity, i.e. $\boldsymbol{\delta u}_x$, $\boldsymbol{\delta u}_y$, $\boldsymbol{\delta u}_z$, scaled with ωR, ωR, and $\langle v \rangle$, respectively, at various cross-sectional positions for $\beta = 20$. Results are given in Figure 5, revealing that the deviations in respective cross-sections of two windows are indeed negligible. Hence, this confirms the applicability of the reoriented cellular flow model for 3-D velocity fields in the RAM.

On the basis of these 3- and 2.5-D velocity field analyses, we can summarize the conclusions as follows:

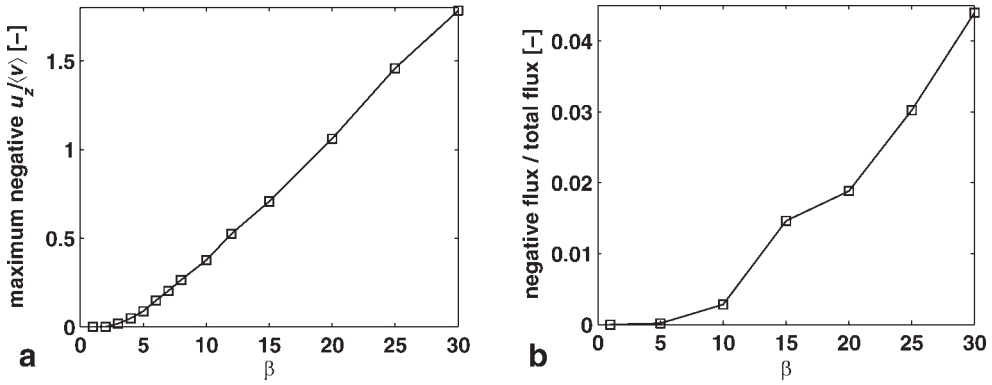

Figure 4. Characterizing back-flows in the RAM.

(a) Effect of increasing β on magnitude of maximum negative $\boldsymbol{u}_z$ scaled with $\langle v \rangle$, and (b) effect of increasing β on negative flux scaled with total flux at the inlet.

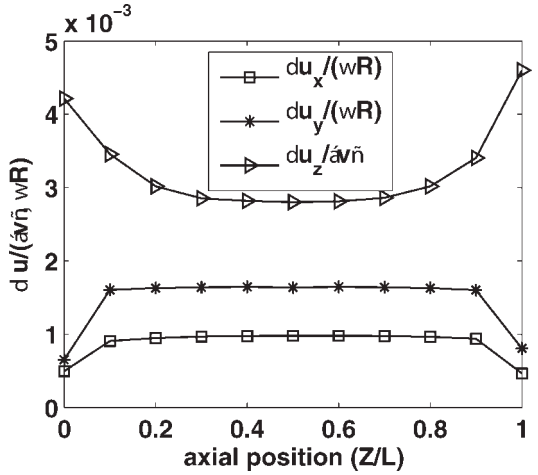

Figure 5. Proof of applicability of cellular flow model in the 3-D flow field of the RAM: comparing velocity field at various cross-sectional positions of two consecutive windows by computing δu (δu_x, δu_y, δu_z).

The velocity at position z of the first window is reoriented by offset angle $\Theta = -36^\circ$ (rotational transformation), and then δu is calculated with respect to the velocity at $z + L + l$ of next neighboring window. The $\delta \boldsymbol{u}_x$ and $\delta \boldsymbol{u}_y$ is scaled with ωR, whereas $\delta \boldsymbol{u}_z$ scaled with $\langle v \rangle$.

• A pronounced coupling exists between axial and transverse components of the velocity field, especially at higher values of β.

• Despite the significant departure of the axial velocity component from the Poiseuille profile at higher values of β, the reoriented cellular flow model is applicable for 3-D flow fields in the RAM.

Now, it is of paramount importance to know whether deviations in the velocity field between 2.5- and 3-D can cause significant differences in mixing patterns. This is investigated in the "Results" section. To this end, we first introduce the mapping method used to study the mixing in the next section.

Methods to Analyze Mixing

Mapping method

Chaotic mixing of viscous liquids in laminar flows is usually based on the situation where the bakers transformation is applied a number of times on a specified volume of material. Spencer and Wiley[17] suggested that the distribution of material in such flows can be handled quite well by the use of matrix methods. The mapping method describes the transport of a conservative quantity from one state to another by means of a mapping matrix, describing the transport of fluid from an initial cross section to a final one (for spatially-periodic flows) or from an initial time to a final time (for time-periodic flows). Numerically, the original mapping method[11–16] exploits the earlier idea as follows: a distribution matrix φ is formed to store information about the distribution of fluid from one discretized cross-section to the next due to a specified flow. To obtain the coefficients of the distribution matrix, the initial cross section of the flow domain is subdivided into a large number of discrete cells (N) of identical size. During flow, the material from a donor cell is transferred to different recipient cells. The fraction of material that is transferred from the donor cell to a recipient cell gives the distribution coefficient of the donor cell with respect to the recipient cell. Thus, in total N cells form a distribution matrix of the order $N \times N$. The discrete coefficient φ_{ij} equals the fraction of deformed sub-domain Ω_j at $z = z_0 + \Delta z$ that is found in the original sub-domain Ω_i at $z = z_0$:

$$\varphi_{ij} = \frac{\int_{\Omega_j|z=z_0+\Delta z \cap \Omega_i|z=z_0} dA}{\int_{\Omega_j|z=z_0|} dA}. \tag{4}$$

Tracking all interfaces of all N cells during a flow over a distance Δz can be done, as we have demonstrated for different flows, but it is cumbersome to track interfaces experiencing complicated deformation patterns. Recently we have formulated an alternative approach to find mapping coefficients that is much simpler to implement.[18,19] Figure 6 depicts how the mapping coefficients are calculated in new formulation of the method. To approximate the coefficients of the mapping matrix (or distribution matrix), K markers inside all cells are tracked. The markers are uniformly distributed in the cells. Then, to determine the final distribution of markers, they are advected during the flow from $z = z_0$ to $z = z_0 + \Delta z$. If the number of markers in the donor cell Ω_j is $\boldsymbol{M_j}$ at $z = z_0$ and the number of markers found after tracking in the recipient cell Ω_i is $\boldsymbol{M_{ij}}$ at $z = z_0 + \Delta z$, then the mapping coefficient $\boldsymbol{\Phi_{ij}}$ is calculated as:

$$\boldsymbol{\Phi}_{ij} = \frac{\boldsymbol{M_{ij}}}{\boldsymbol{M_i}}. \tag{5}$$

In other words, the coefficient $\boldsymbol{\Phi_{ij}}$ is the measure of the fraction of the total flux of cell Ω_j donated to cell Ω_i. If the number of markers tracked is large enough then $\boldsymbol{\Phi_{ij}}$ approaches φ_{ij}.

The elegance of the mapping method is that if one wants to analyze mixing-related scalar quantities, like the concen-

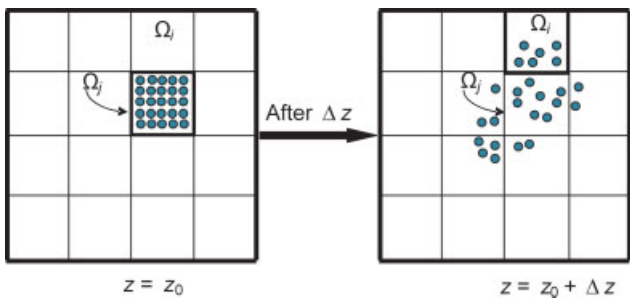

Figure 6. Illustration of the computation of the coefficients Φ_{ij} of the mapping matrix Φ.

The cell Ω_j at $z = z_0$ is covered with a number of markers that are tracked during flow in Δz (to arrive at the final cross section $z = z_0 + \Delta z$). The ratio of the number of markers received by the recipient cell Ω_i to the initial number of markers in Ω_j is determined (in this example $\boldsymbol{\Phi_{ij}}$ is 6/25). [Color figure can be viewed in the online issue, which is available at www.interscience.wiley.com.]

tration vector $\boldsymbol{C} \in \mathrm{IR}^{N \times 1}$ (N is the number of cells) defined on initial cells, then the concentration evolution $\boldsymbol{C^I}$ after the deformation can be obtained by simply multiplying the mapping matrix $\boldsymbol{\Phi}$ with the initial concentration vector $\boldsymbol{C^0}$:

$$\boldsymbol{C}^1 = \Phi \boldsymbol{C}^0. \tag{6}$$

Note that $\boldsymbol{C}$ represents the coarse-grained description of volume fraction (dimensionless concentration) of a marker fluid in a mixture of two marker fluids with identical material properties, and its component C_i describes the concentration (volume fraction) locally averaged in the cell Ω_i. For repetitive mixing, the same operation is repeated multiple times on the same mass and, hence, the concentration evolution after n steps is given by $\boldsymbol{C^n} = \boldsymbol{\Phi^n C^0}$. For sufficiently large n, the matrix $\boldsymbol{\Phi^n}$ will not be sparse and it becomes that large that it can even not be stored anymore. This is due to the fact that after performing the operation n times, material from one cell is advected to a large part of the whole cross section, especially in the case of chaotic advection. Instead of studying $\boldsymbol{\Phi^n}$, the evolution of the concentration after n steps $\boldsymbol{C^n}$ is computed in sequence as follows:

$$\boldsymbol{C}^{i+1} = \boldsymbol{\Phi C}^i, \text{ hence } \boldsymbol{C^n} = \underbrace{(\boldsymbol{\Phi}(\boldsymbol{\Phi}(...(\boldsymbol{\Phi}}_{\text{n times}} \boldsymbol{C}^0)))). \tag{7}$$

Thus, the mapping matrix $\boldsymbol{\Phi}$ is determined only once and is utilized a number of times to study the evolution of concentration in the flow field. Note that the above repetitive multiplication (Eq. 7) brings numerical diffusion in the mapping method. This numerical diffusion is caused by concentration averaging within each cell and depends on two parameters: grid size of mapping and number of mapping steps (n). Reduction in any of the earlier-mentioned factors leads to smaller numerical diffusion in the method.[15] The most important fact is that when comparing various protocols, these two parameters must be fixed. In our simulations, we have used for all optimization study 200 × 200 cells and total number of mapping steps equal to 10 (which is number of windows in RAM). Computation of mapping matrices is expensive, and may take several CPU hours, but, once calculated, the necessary matrix-vector multiplication only takes a few CPU seconds to process the results. The mapping matrix calculations are easily parallelized.[12]

Measure of mixing

To quantify mixing and compare various layouts of the RAM, we employ the flux-weighted discrete intensity of segregation defined in a cross-section, using coarse grain concentration C_i in the mapping cells as a mixing measure (refer Singh et al.[18]):

$$\boldsymbol{I}_{\mathrm{d}} = \frac{1}{\overline{\boldsymbol{C}}\left(1-\overline{\boldsymbol{C}}\right)} \frac{1}{\boldsymbol{F}} \sum_{i=1}^{n} \left(C_i - \overline{\boldsymbol{C}}\right)^2 \boldsymbol{f}_i, \tag{8}$$

where the average concentration $\overline{\boldsymbol{C}}$ is

$$\overline{\boldsymbol{C}} = \frac{1}{\boldsymbol{F}} \sum_{i=1}^{n} C_i \boldsymbol{f}_i, \quad \boldsymbol{F} = \sum_{i=1}^{n} \boldsymbol{f}_i. \tag{9}$$

The term $\boldsymbol{f_i}$ is the volumetric flux through cell number $\boldsymbol{i}$, $\boldsymbol{F}$ is the total flux through the mixer, and N is the number of total cells in the domain. The intensity of segregation $\boldsymbol{I_d}$ is a measure of the deviation of the local concentration from the ideal situation (perfectly mixed case), which represents a homogeneous state of the mixture. In a perfectly mixed system, $\boldsymbol{I_d} = 0$, whereas in a completely segregated system, $\boldsymbol{I_d} = 1$. As found by Galaktionov et al.[13,14] the flux-weighted definition (see Eq. 8) of the intensity of segregation is much better suited for analyzing continuous mixers than area- or volume-averaged definitions of the intensity of segregation. This is due the fact that the real impact of an unmixed island (or chaotic region) in the flow on the quality of mixing is proportional to the flux, carrying this island (or chaotic region).

Defining the mapping matrices of the RAM

For the mapping computations in the RAM, the cross section of interest is covered with a 200 × 200 grid, and each cell is filled with a uniform distribution of 225 (in a 15 × 15 pattern) passive markers (compare with Figure 6). To compute mapping coefficients $\boldsymbol{\Phi_{ij}}$ (Eq. 5) in the 2.5-D approach, the trajectory of markers is tracked by using the axial integration approach. In the axial integration approach, integration is done with respect to the spatial increment along the axial direction, rather than time, eliminating effects of different residence time distributions. This is realized by dividing the transversal velocity components $\boldsymbol{u_x}$ and $\boldsymbol{u_y}$ with the axial velocity component $\boldsymbol{u_z}$:

$$\frac{dx}{dz} = \frac{\boldsymbol{u_x}}{\boldsymbol{u_z}}, \quad \frac{dy}{dz} = \frac{\boldsymbol{u_y}}{\boldsymbol{u_z}}. \tag{10}$$

Note that this approach is only valid for the systems where back flows are not present. In the 2.5-D approach, the axial velocity $\boldsymbol{u_z}$ is always positive in all parts of the RAM (because of Poiseuille profile assumption for this velocity component), and therefore, it is advantageous to use Eq. 10 to track positions of markers. However, the presence of back flow ($\boldsymbol{u_z} < 0$) in the 3-D velocity field of the RAM (see Figure 3) leads to failure of this approach, due to the fact that the back flow makes some material elements in the window to traverse back and later move forward. Therefore, to compute the coefficients of the mapping matrix $\boldsymbol{\Phi_{ij}}$, based on the 3-D velocity field, we apply standard time integration as follows:

$$\frac{dx}{dt} = \boldsymbol{u_x}, \quad \frac{dy}{dt} = \boldsymbol{u_y}, \quad \frac{dz}{dt} = \boldsymbol{u_z}. \tag{11}$$

The time tracking approach, Eq. 11, is computationally more expensive than the axial tracking, Eq. 10, because the parabolic nature of the axial velocity in a channel results in different residence-time distributions for tracers, and therefore, tracers reach their axial final position at different times. In fact, a priori it is unknown the time needed for each particle to reach at the desired spatial position, which requires extra book keeping of particle trajectories. It turned out to be advantageous to use the backward (reverse) particle tracking (BPT) to track the tracers to obtain the mapping coefficients (Eq. 5). In other words, tracers originally filling the recipient

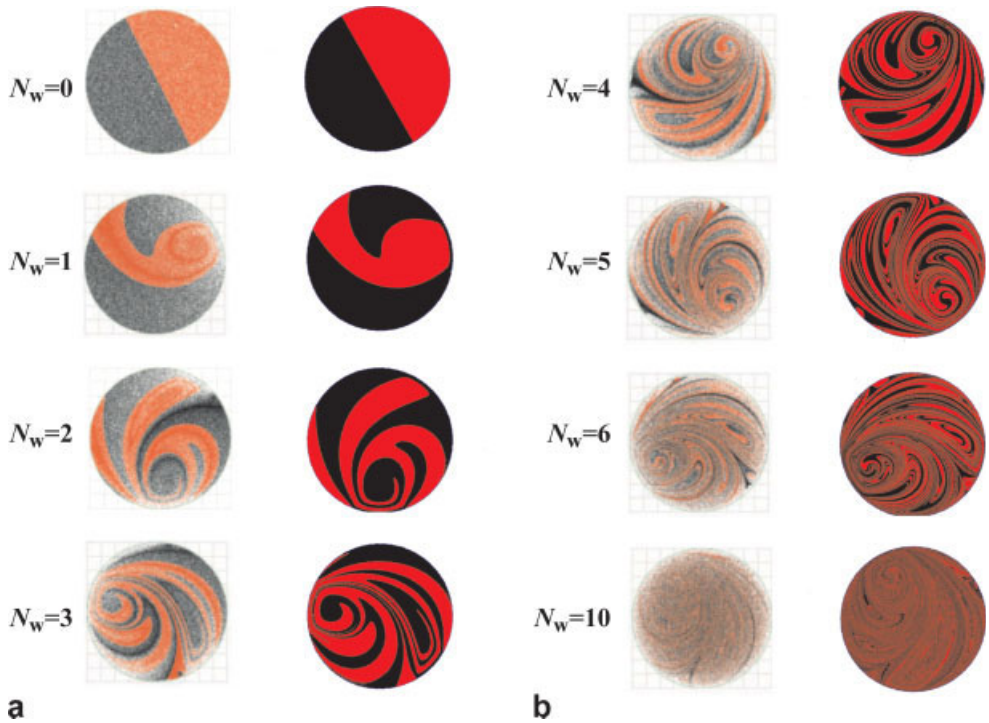

Figure 7. Comparing mixing evolutions obtained by the mapping method [right parts of figure (a) and (b)] with those of Metcalfe et al.[6] [left parts of figure (a) and (b)].

Parameters of simulation are as follows: $\beta = 14$, $\Delta = -45^\circ$, and $\Theta = -108^\circ$. [Color figure can be viewed in the online issue, which is available at www.interscience.wiley.com.]

cell are tracked backward against the flow direction. These equations of motion, Eqs. 10 and 11, are integrated by a fourth-order Runge–Kutta–Bulrish Store scheme with the adaptive step size selection of Press et al.[20] To find the velocity at any arbitrary point, interpolation using the basis function is applied.[12–14] As mentioned earlier, we fix the number of windows of the RAM at $N_w = 10$. To do a full analysis of mixing, one can either compute a single mapping matrix $\mathbf{\Phi}$ representative for the whole RAM to study the final concentration evolution (Eq. 6) or compute 10 individual matrices $\mathbf{\Phi}_i$ ($i = 1, 2,\ldots, 10$) representative for each window of the RAM, and then study the concentration evolution in a sequence (Eq. 7). The matrix $\mathbf{\Phi}$ becomes highly dense especially when the flow is chaotic, while the matrices $\mathbf{\Phi}_i$ ($i = 1, 2,\ldots, 10$) are sparse. Note that the higher i is, the less dense is the respective matrices. Therefore, the matrices $\mathbf{\Phi}_i$ ($i = 1, 2,\ldots, 10$) are more easy to operate (matrix-vector multiplication) and store, which brings a computational advantage. Despite computing 10 mapping matrices still this requires long computation times. The fact that velocity fields (both 2.5- and 3-D) can be computed using reoriented cellular flow approach (it has been found in the "Flow Field Calculations" section that 3-D flow field has the same spatial periodicity as the 2.5-D flow field), it can be utilized to find all distribution of passive tracers, carrying out the integration, Eqs. 10 or 11, only for first window, and subsequently final particle positions for the next windows can be obtained by rotating them by the given offset angle Θ (rotational transformation). In this way, one is required to compute the mapping matrix only for a single window, and then the subsequent matrices can be obtained via the rotation (with the given offset angle Θ), which takes only few CPU seconds. Because in 3-D velocity field any change in offset angle will affect the transition region, therefore, this requires computation of a new velocity field. However, the 2.5-D approach does not take into account transitional effects, and hence various offset angle design of RAM can be analyzed without computing new velocity field. This brings a huge benefit in computational effort and allows various offset angle matrices to be computed very fast for a given opening angle Δ and kinematical parameter β by adopting the 2.5-D approach. This provides an efficient way to predict the optimum offset angle Θ. In this way, the mapping method proves to be a very efficient optimization tool.

Results

Determining the validity range of 2.5-D mixing analyses

First of all, we validate the mapping method results by comparing computed mixing evolutions with the results of Metcalfe et al.[6] (note that both numerical analyses use 2.5-D approach). Figure 7 shows the comparison of mixing after each window, and reveals that the mapping method duplicates mixing evolutions as reported in Metcalfe et al.[6] exactly. Note that Metcalfe et al.[6] validated their numerical dye traces with experimental mixing patterns obtained by same authors, and in turn mapping mixing evolutions are in the agreement with experiment. This demonstrates the suit-

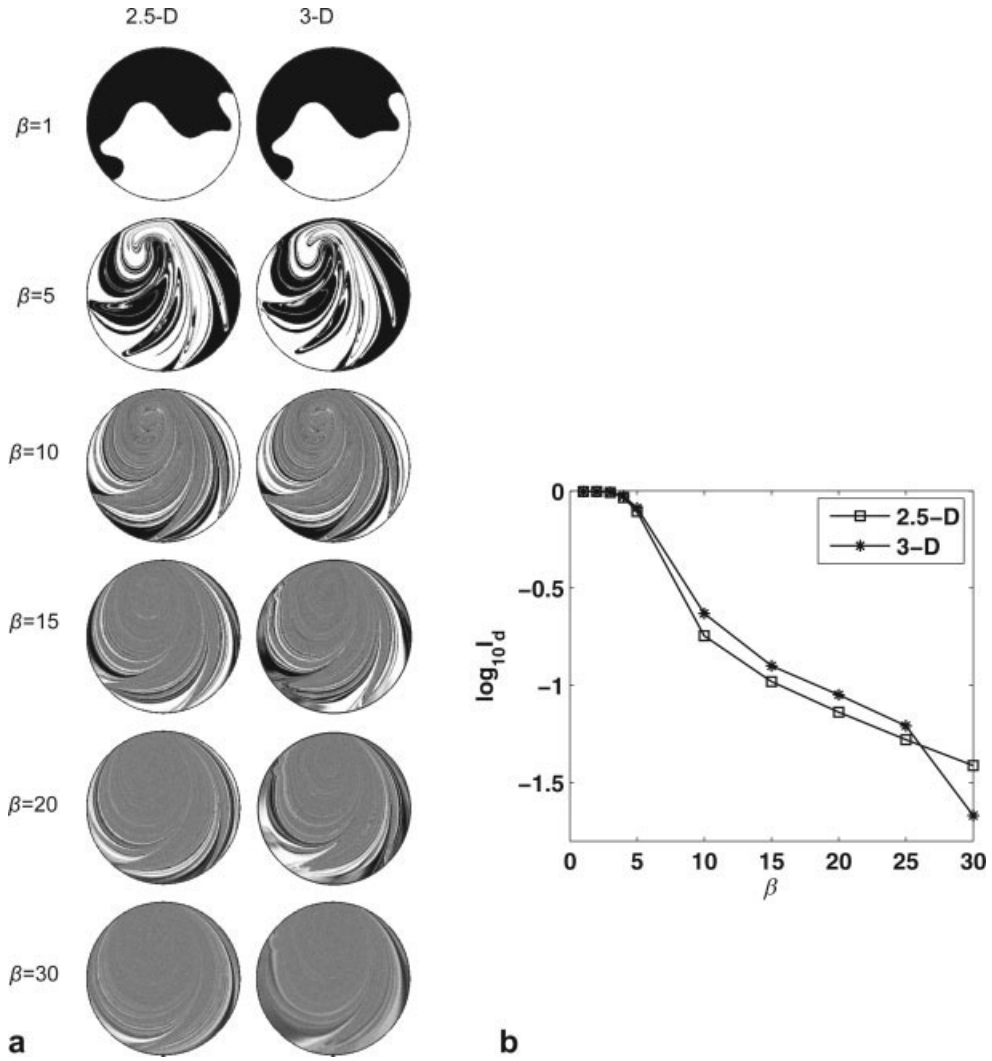

Figure 8. Mixing comparisons obtained via 2.5- and 3-D velocity fields for various values of β after 10 windows of mixing.

(a) Qualitative mixing profiles and (b) intensity of segregation to quantify mixing. The initial concentration pattern $\boldsymbol{C}^0$ contains right half of cross-section filled by black fluid (the geometrical parameters used are as follows: $\Delta = 45^\circ$, $\Theta = -36^\circ$).

ability of the mapping method for 2.5-D mixing analysis of the RAM and in addition, it is important to observe that mapping mixing evolutions show increased level of detail of the mixing structures.

Next we investigate whether the 2.5-D approach is always valid for all designs of the RAM and for all kinematical parameter range. The 3-D flow fields reveal that the effects of the transition region present between two consecutive windows are quite significant (see "Flow Field Calculations" section) especially at higher values of β, and hence we expect differences in the mixing profiles obtained by both (2.5- and 3-D) velocity fields. To find those differences, we performed detailed mixing analyses in mixers with different designs based on both the 2.5- and 3-D velocity fields. First, we start comparing mixing in the design with a negative offset $\Theta = -36^\circ$, and then we discuss mixing in the design with a positive offset $\Theta = 36^\circ$ (see "Flow Field Calculations" section for 3-D velocity field). Results of mixing are computed for $\beta = 1, 2, \ldots, 5, 10, 15, 20, 25$, and 30 using both the 2.5- and 3-D approaches. To study the concentration evolution here, we compute the mapping matrix $\boldsymbol{\Phi}$ for the total flow domain to avoid errors associated with numerical diffusion that is intrinsic to the mapping method.[15] Figure 8a shows the evolutions of mixing obtained after 10 windows for the various values of β, and Figure 8b depicts the quantitative comparison of mixing using the flux-weighted intensity of segregation I_d. The differences between the 2.5- and 3-D mixing results are insignificant in this range of parameters. Other general conclusions are that mixing is poor for $\beta < 5$, whereas for $\beta > 5$, it shows a sharp decrease in intensity of segregation with β, revealing the onset of chaos above this value of β. This implies that one needs a minimum value of β to achieve chaotic mixing, which is consistent with other studies on the RAM (see refs. 6 and 7).

To investigate the differences in mixing profiles after each window, we show here the mixing profiles obtained by both

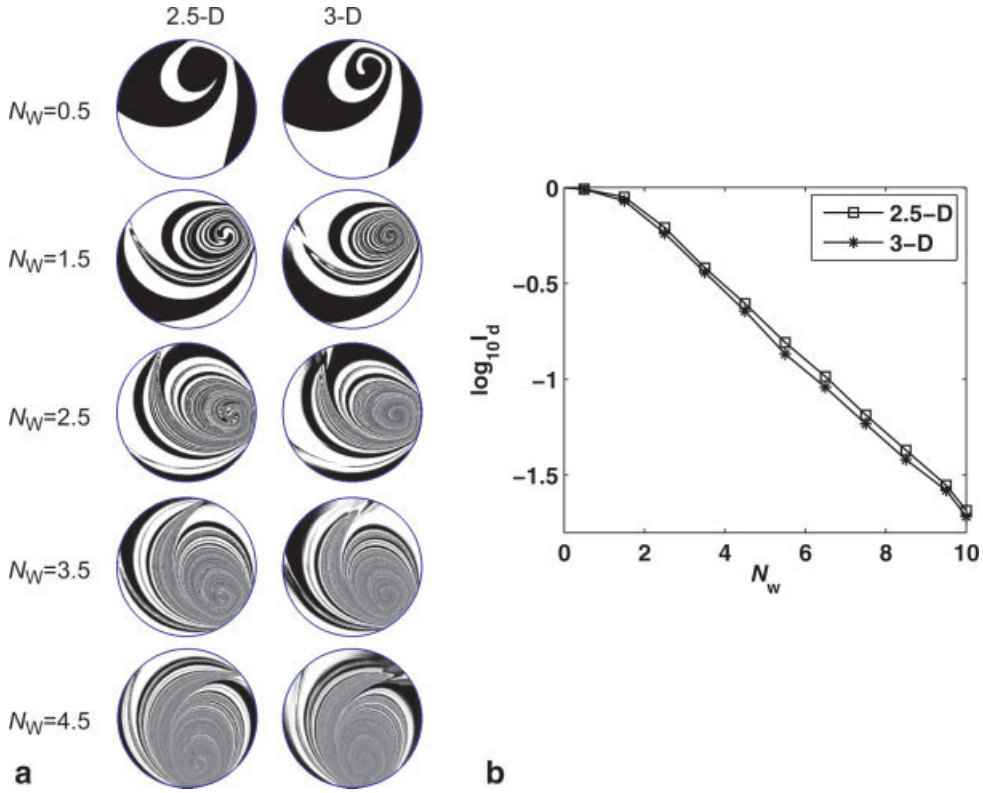

Figure 9. 2.5-D vs. 3-D: window to window comparison of mixing for β = 30, (a) qualitative mixing profiles, and (b) flux-weighted intensity of segregation to quantify mixing (Δ = 45°, Θ = −36°).

[Color figure can be viewed in the online issue, which is available at www.interscience.wiley.com.]

approaches (2.5- and 3-D) at the respective windows, as shown in Figure 9 for β = 30. We choose the highest value of β because velocity field analyses suggest higher deviations between 2.5- and 3-D velocity fields (see Figure 3). Because in the 3-D flow field, back flow is present at the end cross-sections of each window (which causes some particle trajectories to intersect the cross section more than once), mixing evolutions are computed at the mid cross-section of each window where back flow is absent. The resulting mixing evolution (see Figure 9a) reveals some differences in patterns of 2.5- and 3-D at the beginning of mixing (N_w = 0.5, 1.5; here 0.5 is used to represent the mid cross-section of a window). However, at the later stages of mixing, the differences prove to be small. The quantitative characterization in Figure 9b also reveals that the differences between two cases are insignificant.

Next, we discuss the differences in mixing profiles for the design with positive offset angle Θ = 36°. Figure 10 shows the mixing evolutions obtained by using the 2.5- and 3-D flow fields, and opposed to the results of the negative offset (Θ = −36°), in this case we see clear differences, especially at higher values of β. The numbers of unmixed islands in the 2.5-D mixing profiles are more than those in 3-D results at higher values of β (>10). We observe a significant effect of the transition regions and back flow on the resulting mixing profiles, which leads to locally better mixing by reducing the number of KAM boundaries (poor mixing regions). However, this local enhancement in mixing never leads to globally chaotic mixing irrespective of the β value. In both 2.5- and 3-D approaches, the KAM boundaries are always present for the positive offset design irrespective of the value of β, and number of windows involved. This phenomenon has already been observed experimentally by Metcalfe et al.,[6] where they found that positive offset designs are poor candidates for chaotic mixing. Speetjens et al.[7] found on the basis of fundamental symmetry analysis of the flow field in a RAM (2.5-D) that only in the case of negative offset designs there exists period doubling bifurcations, which is the route to chaos in the mixing operations. Interesting is that as β increases from 20 to 30, mixing deteriorates, as opposed to the negative offset design where quality of mixing always increases with increasing β (see Figure 8). This is most probably due to reappearance of some KAM boundaries. In spite of huge differences in mixing patterns of 2.5- and 3-D approaches for Θ = 36°, both approaches show same trend in mixing quality, for example existence of an optimum β for accomplishing best mixing (see Figure 10). Overall, concerning the differences between 3- and 2.5-D analyses, we can conclude the following:

- In mixer designs with negative offset angle, $\Theta < 0$, the differences between 2.5- and 3-D are insignificant, whereas mixing continues to improve with the increase of β.
- In designs with positive offset angle $\Theta > 0$, the differences are significant, especially at higher values of β (>10). But, overall mixing is poor, leaving unmixed islands in the flow domain, because KAM boundaries exist and mixing deteriorates at high values of β (>20).

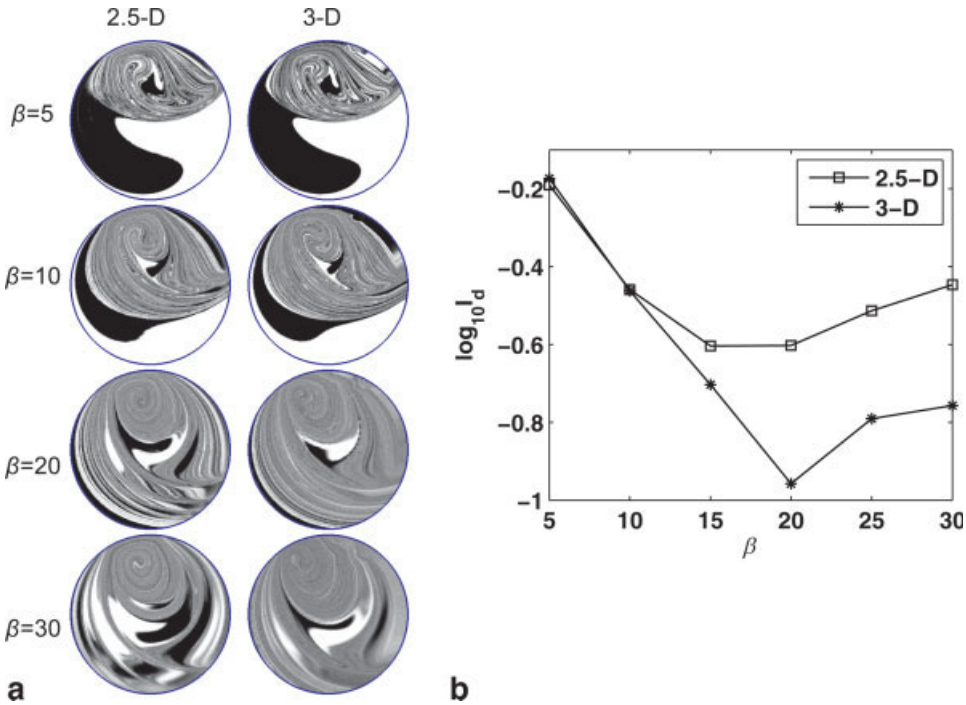

Figure 10. 2.5-D vs. 3-D: effect of positive offset (+Θ) on the mixing evolutions after 10 windows of mixing at various values of β.

(a) Qualitative mixing patterns (b) flux-weighted intensity of segregation to quantify mixing. The initial concentration pattern C^0 contains right half of cross-section filled by black fluid (the geometrical parameters used are: $\Delta = 45^\circ$, $\Theta = 36^\circ$). [Color figure can be viewed in the online issue, which is available at www.interscience.wiley.com.]

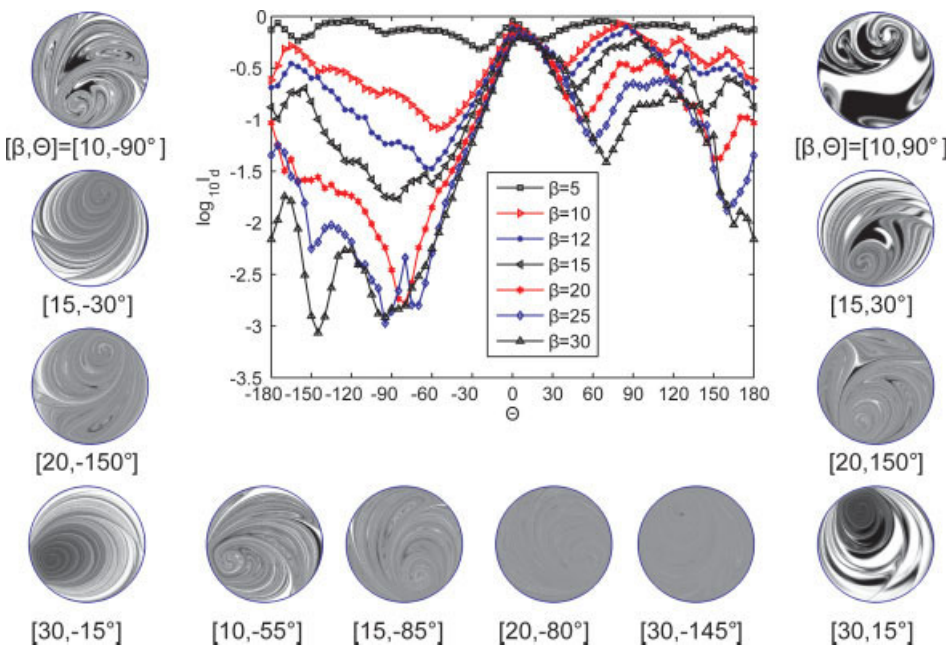

Figure 11. Optimum offset angle Θ for an opening angle $\Delta = -45^\circ$ for various values of β: qualitative mixing profiles at few chosen values of [β, Θ], and flux-weighted intensity of segregation to quantify mixing.

The initial concentration pattern C^0 contains right half of cross-section filled by black fluid. [Color figure can be viewed in the online issue, which is available at www.interscience.wiley.com.]

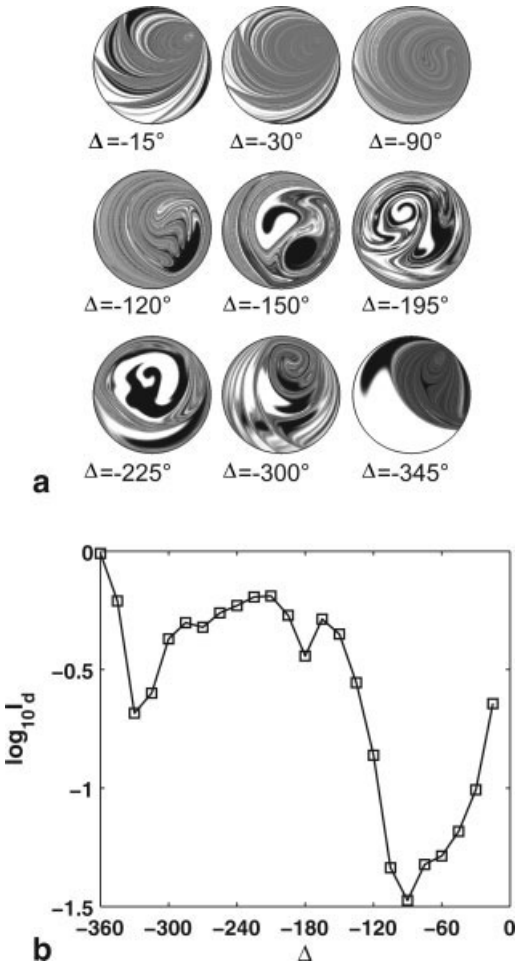

Figure 12. Effect of opening angle Δ on mixing evolution in the RAM.

(a) Qualitative mixing patterns, (b) flux-weighted intensity of segregation to quantify mixing. The initial concentration pattern C^0 contains right half of cross-section filled by black fluid ($\Theta = -35^\circ$, $\beta = 20$, and $N_w = 10$).

This confirms that to achieve good mixing in the RAM, designs with negative offset, Θ (<0) have to be chosen, and optimization for these designs can be performed in an accurate way using the 2.5-D flow field. However, the 2.5-D approach can be used for designs with positive offset Θ (>0) to get one estimate of qualitative trend of optimum design parameters.

Optimization of the RAM

To predict the best design of the mixer requires to analyze the complete range of geometrical and kinematical parameters [Θ, Δ, β] of the mixer, where Θ lies in the range of [-180°, 180°], Δ lies in the range [-360°, 0°], and β lies in the range [0, 30]. This huge parameter space leads to numerous cases to be analyzed to predict the optimum. However, three facts allow this optimization problem to be solved efficiently. First, the 2.5-D flow field is suited to accurately capture mixing in the mixer with negative offset designs, whereas mixing analyses in positive offset designs show the same trend when compared with 3-D (see Figure 10). Second, the mapping method is capable in studying concentration evolutions efficiently. Third, the reoriented duct flow model allows to integrate particle tracks only once for a single window to obtain a mapping matrix, and later these particle tracks can simply be rotated by the offset angle Θ to obtain mapping matrices for consecutive windows. We give an example: to find the best offset angle for $\Delta = -45^\circ$, take small step $\delta\Theta = 5^\circ$ (because mixing is highly sensitive for the values of Θ), at various values of β as shown in Figure 11. Despite the presence of some local minima the intensity of segregation plot reveals the existence of a global optimum offset angle where mixing is the best (for the design with $\Delta = -45^\circ$), slightly depending on β. A design with $\Theta \approx -90^\circ$ seems a perfect compromise for all β values investigated.

Now we investigate the best choice of the opening angle Δ of the window for a $\Theta = -35^\circ$ considering the range of $\Delta\ -360^\circ \leq \Delta \leq 0^\circ$ with steps of $\delta\Delta = 15^\circ$. The mixing is always of inferior quality when Δ is below -180°, see Figure 12, and a relatively sharp optimum $\Delta \approx -90^\circ$ is found in the range [-180°, 0°]. Therefore, for full optimization of parameter space of the RAM, we consider only the range [-180°, 0°] for Δ.

Now the last task is to achieve a complete optimized set of parameters, and this requires investigation of the whole parameter space. Figure 13 shows complete optimization results, both in 3-D surface plots and 2-D contour plots, for a number of values of β, and on the basis of these plots, we report the optimum design parameters in Table 1 at various values of β.

From these plots, the most important conclusions of this optimization study can be summarized as follows:

- The optimum opening angle Δ always lies in the range [-90°,-45°].
- The optimum offset angle Θ always lies below -60°.
- These optimum design parameters show a slight dependence on the kinematic parameter β.
- Choosing $\Delta = -60^\circ$ and $\Theta = -90^\circ$ is close to all precise optimum values and rather good choice for the design parameter of the RAM for all values of the kinematical parameter β.

Conclusions

A detailed analysis of mixing in the RAM has been performed to achieve a complete set of optimized design parameters. The large range of geometrical and kinematical parameters, the offset angle Θ, the opening angle Δ and the dimensionless kinematical parameter β, respectively, necessitates analysis of many cases. Conventional analyses based on particle tracking, e.g., Poincaré sections, numerical dye traces, stretching distributions, and residence time distributions are cumbersome to analyze the whole parameter space. In this regard, we have demonstrated a fast methodology to analyze the parameter space in an efficient way using the mapping method. Two types of flow fields are used: a 2.5-D model where the transverse components of velocity are taken from an analytical solution from the literature and assuming a Poiseuille profile for axial flow (2.5-D approach), and a full 3-D model where the velocity field is obtained numerically. A significant difference between 3- and 2.5-D flow fields

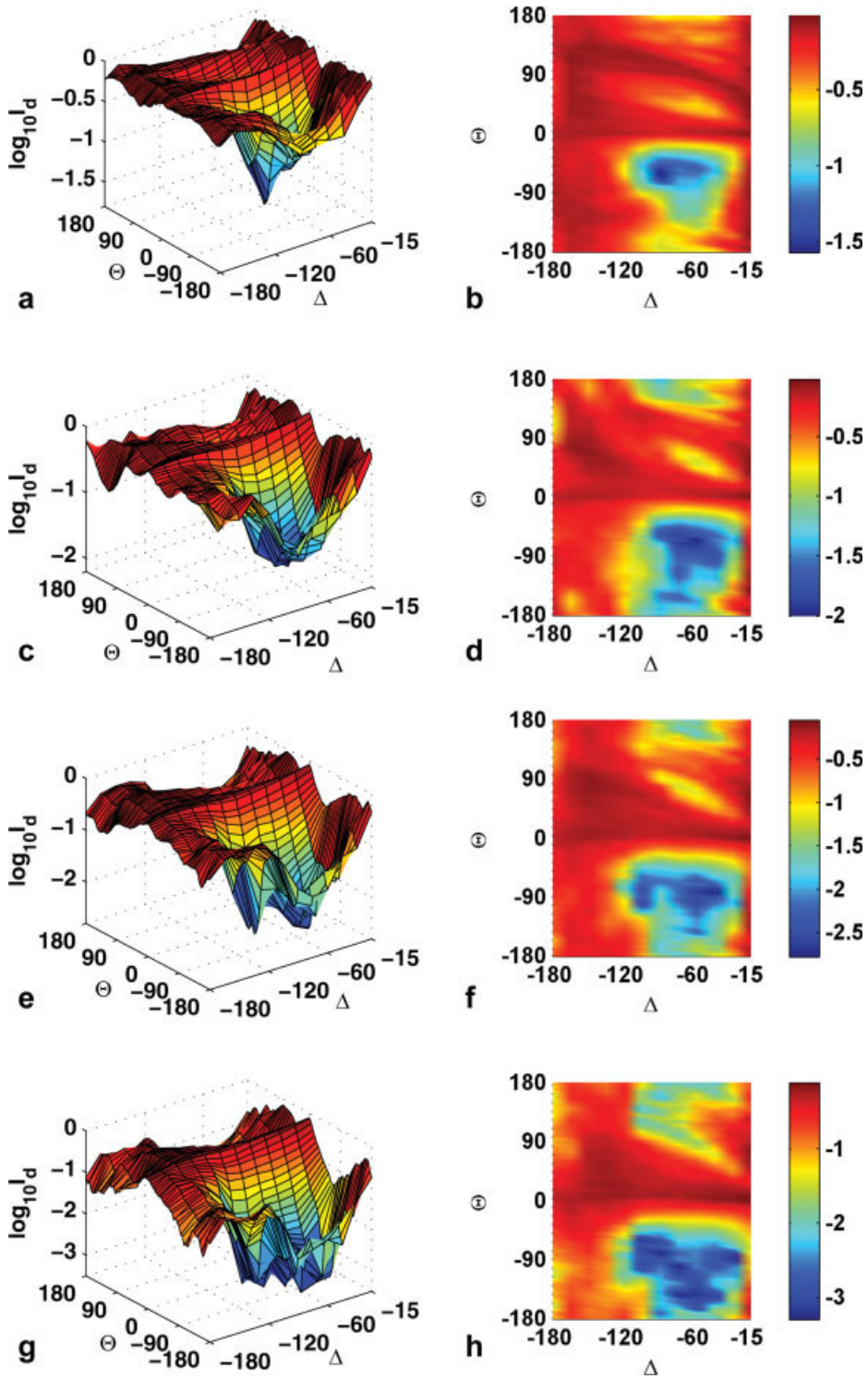

Figure 13. Optimizing the RAM.

Logarithm of intensity of segregation is plotted as function of the offset angle Θ and opening angle Δ for $\beta = 10$, 15, 20, and 30. Left side of this figure shows a 3-D surface plot, and right side shows a 2-D contour plot, the kinematical parameter β value for figures (a) and (b) $\beta = 10$, (c) and (d) $\beta = 15$, (e) and (f) $\beta = 20$, and (g) and (h) $\beta = 30$. [Color figure can be viewed in the online issue, which is available at www.interscience.wiley.com.]

Table 1. Optimum Design Parameters Δ and Θ of the RAM for Various Values of the Kinematical Parameter β

β	Δ	Θ	I_d
5	−90	−140	0.31376
10	−90	−60	0.02689
12	−75	−65	0.01399
15	−60	−65	0.00994
20	−45	−80	0.00166
25	−60	−145	0.00095
30	−75	−100	0.0005

exist especially at higher values of β, leading to pronounced coupling in velocity components. This is evident by the presence of back flow and deviations from Poiseuille profile along a window of the RAM. In spite of significant differences between both flow fields, the reoriented duct flow model is found to be valid also for the 3-D flow field. This is advantageous, because this implies that tracking of passive particles is only needed for the first window to find a mapping matrix, and remaining matrices for consecutive windows simply follow from rotation of the tracked co-ordinates of passive particles for first window. This is computationally very fast and formed the basis for the optimization of the offset angle Θ for a given Δ and β.

The comparison of mixing profiles obtained by the mapping method, using both the 2.5- and the 3-D flow fields, reveal that the 3-D effects on mixing profiles are found to be negligible in designs that lead to chaotic mixing, whereas significant differences are found in the designs that lead to poor mixing. In the RAM, a design with positive offset, $\Theta > 0$, always leads to poor mixing, due to presence of KAM boundaries irrespective of β, whereas a design with negative offset, $\Theta < 0$, is a candidate for chaotic mixing (if the value of β is sufficient). This confirmed that the mixing analyses using the 2.5-D approach are suitable to analyze mixing in designs with negative offset. The reoriented cellular flow model, the availability of analytically known velocity components in the 2.5-D approach, and the capability of the mapping method to study concentration evolutions, proved very efficient to allow efficient searching of the complete range of design and kinematical parameter [Θ, Δ, β] space. The optimization study of the RAM performed with this method reveals that for all the values of kinematical parameter β the optimum design parameters are an opening angle $\Delta = -60^\circ$ and an optimum offset angle $\Theta = -90^\circ$.

Acknowledgments

The authors acknowledge T.G. Kang for his fruitful discussions. They highly appreciate all information on the RAM that was kindly provided by G. Metcalfe and M. Rudman of CSIRO, Australia. They are also grateful to the Dutch Polymer Institute (DPI) for financial support (grant no. 446).

Literature Cited

1. Aref H. Stirring by chaotic advection. *J Fluid Mech*. 1984;143:1–21.
2. Ottino JM. *The kinematics of Mixing: Stretching, Chaos, and Transport*. Cambridge: Cambridge University Press, 1989.
3. Middleman S. *Fundamentals of Polymer Processing*. New York: McGraw-Hill, 1977.
4. Sluijters R. Het principe van de multiflux menger. *De Ingenieur, Chemische Techniek 3*. 1965;77:Ch 33–36.
5. Pahl MH, Muschelknautz E. Static mixers and their applications. *Chemie Ingenieur Technik*. 1980;52:285–291.
6. Metcalfe G, Rudman M, Brydon A, Graham L, Hamilton R. Composing chaos: an experimental and computational study of an open duct mixing flow. *AIChE J*. 2006;52:9–28.
7. Speetjens M, Metcalfe G, Rudman M. Topological mixing study of non-Newtonian duct flows. *Phys Fluid*. 2006;18:103103.
8. Speetjens M, Rudman M, Metcalfe G. Flow regime analysis of non-Newtonian duct flows. *Phys Fluid*. 2006;18:013101.
9. Hwu TH, Young DL, Chen YY. Chaotic advections for stokes flows in circular cavity. *J Eng Mech*. 1997;123:774–782.
10. Meleshko VV, Galaktionov OS, Peters GWM, Meijer HEH. Three-dimensional mixing in stokes flow: the partitioned pipe mixer problem revisited. *Eur J Mech B/Fluids*. 1999;18:783–792.
11. Anderson PD, Meijer HEH. Chaotic mixing analyses by distribution matrices. *App Rheol*. 2000;10:119–133.
12. Galaktionov AS, Anderson PD, Peters GWM. Mixing simulations: tracking strongly deforming fluid volumes in 3D flows. In: Bubak M, Dongarra J, Wasniewski J, editor. *Lecture notes in computer science. Vol. 1332: Recent Advances in Parallel Virtual Machine and Message Passing Interface*. New York: Springer. 1997:463–469.
13. Galaktionov OS, Anderson PD, Peters GWM, Meijer HEH. Morphology development in Kenics static mixers (application of the extended mapping method). *Can J Chem Eng*. 2002;80:604–613.
14. Galaktionov OS, Anderson PD, Peters GWM, Meijer HEH. Analysis and optimization of Kenics mixers. *Int Polym Proc*. 2003;XVIII:138–150.
15. Kruijt PGM, Galaktionov OS, Anderson PD, Peters GWM, Meijer HEH. Analyzing mixing in periodic flows by distribution matrices: mapping method. *AIChE J*. 2001;47:1005–1015.
16. Kruijt PGM, Galaktionov OS, Peters GWM, Meijer HEH. The mapping method for mixing optimization. II. Transport in a corotating twin screw extruder. *Int Polym Proc*. 2001;XVI:161–171.
17. Spencer R, Wiley R. The mixing of very viscous liquids. *J Colloid Sci*. 1951;6:133–145.
18. Singh MK, Kang TG, Meijer HEH, Anderson PD. The mapping method as a toolbox to analyze, design and optimize micromixers. *Microfluidics Nanofluidics*. 2008;5:313–315.
19. Kang TG, Singh MK, Kwon TH, Anderson PD. Chaotic mixing using periodic and aperiodic sequences of mixing protocols in a micromixer. *Microfluidics Nanofluidics*. 2008;4:589–599.
20. Press WH, Teukolsky SA, Vetterling WT, Flannery BP. *Numerical Recipes in FORTRAN*. New York: Cambridge University Press, 1992.

Manuscript received Jan. 14, 2008, and revision received May 5, 2008.